

COHERENT LOCAL EXPLANATIONS FOR MATHEMATICAL OPTIMIZATION

Anonymous authors

Paper under double-blind review

ABSTRACT

The surge of explainable artificial intelligence methods seeks to enhance transparency and explainability in machine learning models. At the same time, there is a growing demand for explaining decisions taken through complex algorithms used in mathematical optimization. However, current explanation methods do not take into account the structure of the underlying optimization problem, leading to unreliable outcomes. In response to this need, we introduce Coherent Local Explanations for Mathematical Optimization (CLEMO). CLEMO provides explanations for multiple components of optimization models, the objective value and decision variables, which are coherent with the underlying model structure. Our sampling-based procedure can provide explanations for the behavior of exact and heuristic solution algorithms. The effectiveness of CLEMO is illustrated by experiments for the shortest path problem, the knapsack problem, and the vehicle routing problem.

1 INTRODUCTION

The field of mathematical optimization plays a crucial role in various domains such as transportation, healthcare, communication, and disaster management (Petropoulos et al., 2024). Since 1940s, significant advancements have been made in this field, leading to the development of complex and effective algorithms like the simplex method and the gradient descent algorithm (Nocedal & Wright, 2006). More recently, the integration of artificial intelligence (AI) and machine learning (ML) techniques has further enhanced optimization methods (Bengio et al., 2021; Scavuzzo et al., 2024).

When using mathematical optimization in practical applications, decision makers must come to a consensus on the *main components* of the optimization model such as decision variables, objective function, and constraints. Afterwards, they need to employ an exact or heuristic algorithm to solve the resulting problem. For setting up the model, the decision maker has to accurately estimate all necessary parameters for the model and algorithm, *e.g.*, future customer demands or warehouse capacities. However, the solution algorithm can be highly sensitive to even small deviations in these parameters and inaccurate parameter estimations can result in sub-optimal decisions being made.

The analysis of the behavior of an optimization model regarding (small) changes in its problem parameters is widely known as *sensitivity analysis* (Borgonovo & Plischke, 2016) or *parametric optimization* (Still, 2018). In both areas, many methods were developed to analyze the model behavior locally and globally, *e.g.*, by one-at-a-time methods, differentiation-based methods or variance-based methods (Borgonovo & Plischke, 2016; Iooss & Lemaître, 2015; Razavi et al., 2021). One of the promising directions mentioned in (Razavi et al., 2021) is the use of ML models to develop sensitivity analysis methods. The main idea of such an approach is to fit an explainable ML model which locally approximates the behavior of the component of the optimization problem to be analyzed (like the optimal objective function value); see *e.g.*, (Wagner, 1995). Usually, linear regression models are fitted because the standardized regression coefficient becomes a natural sensitivity measure. This approach is similar to the LIME method, which is widely used to explain trained ML models (Ribeiro et al., 2016).

Although ML-based sensitivity analysis is effective and model-agnostic, it falls short in providing clear explanations to users when analyzing various components of a model at the same time. Decision makers often need to analyze the main components of an optimization model, such as the objective function value and the values of the decision variables, which are closely intertwined due to the

054 problem’s structure. However, fitting separate linear models to predict the outcome of each component
 055 disregards this correlation and leads to incoherent explanations. This can result in situations where
 056 either (i) the predicted optimal value does not align with the objective value of the predicted solution,
 057 or (ii) the predicted solution violates the constraints of the problem. Inconsistent predictions that do
 058 not align with the model’s structure do not enhance understanding of the optimization model; instead,
 059 they can cause confusion for the decision makers. To illustrate this, consider the following simple
 060 optimization model

$$061 \max\{x_1 + x_2 : 4x_1 + 4.1x_2 \leq 10, x_1 \geq 0, x_2 \geq 0\}.$$

062
 063 Suppose that the coefficient $a_{12} = 4.1$ is the sensitive parameter to analyze. The decision maker
 064 is seeking to understand the impact that small changes in this parameter will have on the optimal
 065 decision values x_1^*, x_2^* . Fitting two separate linear models on a small number of samples for a_{12}
 066 leads to the approximations $x_1^* \approx 0.11a_{12}$ and $x_2^* \approx 0.59a_{12}$. If we apply the latter predictions to
 067 our nominal parameter value of $a_{12} = 4.1$, then the constraint value becomes

$$068 4 \cdot 0.11a_{12} + 4.1 \cdot 0.59a_{12} \approx 11.7 > 10,$$

069
 070 which has a constraint violation of more than 17%. While the fitted linear models are explainable
 071 approximations of our problem components, they are not coherent and hence do not provide reliable
 072 explanations to the user.

073 **Contributions.** In this work, we present a new sampling-based approach called Coherent Local
 074 Explanations for Mathematical Optimization (CLEMO). This approach extends the concept of local
 075 explanations to multiple components of an optimization model that are *coherent* with the structure of
 076 the model. To incorporate a measure of coherence, we design regularizers evaluating the coherence
 077 of the explanation models. We argue that CLEMO is method-agnostic, and hence, it can be used
 078 to explain arbitrary exact and heuristic algorithms for solving optimization problems. Lastly, we
 079 empirically validate CLEMO on a collection of well-known optimization problems including the
 080 shortest path problem, the knapsack problem, and the vehicle routing problem. Our evaluation focuses
 081 on fidelity, interpretability, coherence, and stability when subjected to resampling.

082 **Related literature.** Recently, there has been a significant amount of research focused on improving
 083 the explainability of ML models (Adadi & Berrada, 2018; Bodria et al., 2023; Dwivedi et al., 2023;
 084 Linardatos et al., 2021; Minh et al., 2022; Das & Rad, 2020). Common XAI methods include
 085 feature-based explanation methods that fit interpretable surrogate models, such as LIME (Ribeiro
 086 et al., 2016). When LIME is applied under specific conditions, including binary input features and a
 087 linear surrogate, it can recover Shapley values (Lundberg & Lee, 2017). LIME was analyzed and
 088 extended in several works regarding its stability (Zhang et al., 2019; Zafar & Khan, 2021) or its use
 089 of advanced sampling techniques (Zhou et al., 2021; Saito et al., 2021). In (Dieber & Kirrane, 2020),
 090 interviews were conducted with individuals that never worked with LIME before. The research
 091 shows that LIME increases model interpretability although the user experience could be improved.
 092 Other XAI methods are example-based explanations, such as counterfactual explanations, see *e.g.*,
 093 the survey by Guidotti (2024).

094 Recently, the notion of explainable and interpretable mathematical optimization attained increasing
 095 popularity. Example-based explanation methods such as counterfactuals were introduced to explain
 096 optimization models. Korikov et al. (2021) and Korikov & Beck (2023) examine counterfactual
 097 explanations for integer problems using inverse optimization. Generalizations of the concept have also
 098 been investigated theoretically and experimentally for linear optimization problems and it has been
 099 found that even for simple linear problems this problem is NP-hard (Kurtz et al., 2025). For integer
 100 optimization problems, the becomes even more complex, it is Σ_2^P -hard as shown by Engelhardt et al.
 101 (2025). Furthermore, counterfactuals for data-driven optimization were studied by Forel et al. (2023).
 When heuristics are used, there is no known method to compute counterfactuals.

102 A different approach is incorporating interpretability into the optimization process resulting in
 103 intrinsic explainable decision making contrary to the post-hoc explanation method. In Aigner et al.
 104 (2024), for example, the authors study optimization models with an explainability metric added to
 105 the objective resulting in a optimization model that makes a trade-off between optimality and
 106 explainability. Similarly in Goerigk & Hartisch (2023), the authors ensure an interpretable model by
 107 using decision trees that resemble the optimization process and hence explain the model by providing
 optimization rules based on the model parameters.

While -to the best of our knowledge- feature-based explanation methods are scarce for mathematical optimization, parametric optimization and sensitivity analysis are strongly related to these methods. In both fields, the effect of the problem parameters on the model’s output is analyzed where the model’s output can be the optimal value, optimal decision values or even the runtime of the algorithm; see Still (2018); Borgonovo & Plischke (2016); Iooss & Lemaitre (2015); Razavi et al. (2021). Three decades ago, Wagner (1995) already presented a global sensitivity method in which he approximated the optimal objective value of linear programming problems like the knapsack problem with a linear regression model. For this, he used normal perturbations of the model parameters as an input, somewhat a global predecessor of LIME.

2 PRELIMINARIES

We write vectors in boldface font and use the shorthand notation $[n]_0 := \{0, \dots, n\}$ and $[n]_1 := \{1, \dots, n\}$ for the index sets.

LIME. Local Interpretable Model-agnostic Explanations (LIME) is an XAI method to produce an explanation for black-box ML models $\bar{h} : \mathcal{Z} \rightarrow \mathbb{R}$, which map any data point z in the data space \mathcal{Z} to a real value. Given a data point z^0 , LIME approximates \bar{h} locally around this point with a surrogate model \bar{g} from a set of explainable models \mathcal{G} (e.g., linear models, decision trees). To this end, LIME samples a set of points z^1, \dots, z^N in proximity to z^0 and calculates an optimizer of the problem

$$\arg \min_{\bar{g} \in \mathcal{G}} \sum_{i=0}^N w^i \ell(\bar{g}(z^i), \bar{h}(z^i)) + \Omega(\bar{g}), \quad (1)$$

where ℓ is a fidelity loss function, Ω is a complexity measure and w^i weighs data points according to their proximity to z^0 . LIME uses an indicator function as a complexity measure returning 0 when the number of non-zero features used by \bar{g} is at most K , and ∞ , otherwise. For the weights, LIME uses $w^i = \exp(-d(z^i, z^0)^2/\nu^2)$ with distance function d and hyperparameter ν .

Mathematical Optimization. In mathematical optimization, the aim is to optimize an objective function over a set of feasible solutions. Formally, an optimization problem is given as

$$\begin{aligned} \min \quad & f(\mathbf{x}; \boldsymbol{\theta}) \\ \text{s.t.} \quad & \mathbf{x} \in \mathbb{X}(\boldsymbol{\theta}), \end{aligned} \quad (2)$$

where $\mathbf{x} \in \mathbb{R}^p$ are the decision variables, f is an objective function which is parameterized by parameter vector $\boldsymbol{\theta} \in \Theta \subseteq \mathbb{R}^q$ and $\mathbb{X}(\boldsymbol{\theta}) \subseteq \mathbb{R}^p$ is the feasible region, again parameterized by $\boldsymbol{\theta}$. We call $\boldsymbol{\theta}$ the optimization parameters. As an example, one popular class of problems belongs to linear optimization, where the problem is defined as $\min\{\mathbf{c}^\top \mathbf{x} : \mathbf{A}\mathbf{x} = \mathbf{b}, \mathbf{x} \geq \mathbf{0}\}$. In this case, we have $\boldsymbol{\theta} = (\mathbf{c}, \mathbf{A}, \mathbf{b})$, $f(\mathbf{x}; \boldsymbol{\theta}) = \mathbf{c}^\top \mathbf{x}$, and $\mathbb{X}(\boldsymbol{\theta}) = \{\mathbf{x} \geq \mathbf{0} : \mathbf{A}\mathbf{x} \geq \mathbf{b}\}$. The most popular methods to solve linear optimization problems are the simplex method or the interior point method (Bertsimas & Tsitsiklis, 1997).

Many real-world applications from operations research involve integer decision variables. In this case the feasible region is given as $\mathbb{X}(\boldsymbol{\theta}) = \{\mathbf{x} \in \mathbb{Z}^p : \mathbf{A}\mathbf{x} \geq \mathbf{b}\}$. Such so called linear integer optimization problems are widely used, for example for routing problems, scheduling problems and many others (Petropoulos et al., 2024). The most effective exact solution methods are based on branch & bound type algorithms (Wolsey, 2020). However, due to the NP-hardness of this class of problems often large-sized integer problems cannot be solved to optimality in reasonable time. Hence, often problem-specific or general purpose heuristic algorithm are used to quickly calculate possibly non-optimal feasible solutions.

3 METHODOLOGY

In this section, we present CLEMO, a novel method to provide coherent local explanations for multiple components of mathematical optimization problems. Consider a given instance of problem (2) which is parametrized by $\boldsymbol{\theta}^0$, and we call it the *present problem*. Additionally, we have a solution algorithm $h : \Theta \rightarrow \mathbb{R}^{p+1}$ that we want to explain. The algorithm calculates feasible solutions for every problem instance of problem (2) and returns an objective value and a decision vector as components of the optimization model by $h(\boldsymbol{\theta}) := (f(\mathbf{x}; \boldsymbol{\theta}), \mathbf{x})$. Note that this algorithm does not necessarily have to

return an optimal solution, since our method also works for heuristic or approximation algorithms. The two components we aim to explain in this work are (i) the optimal objective value, and (ii) the values of the decision variables. To this end, we fit $p + 1$ explainable models combined in the vector-valued function $g : \Theta \rightarrow \mathbb{R}^{p+1}$ where $g(\boldsymbol{\theta}) = (g_f(\boldsymbol{\theta}), g_{x_1}(\boldsymbol{\theta}), \dots, g_{x_p}(\boldsymbol{\theta}))$. Here, Θ is the parameter space containing all possible parameter vectors $\boldsymbol{\theta}$ for problem (2). For example, the model g_{x_i} ideally maps every parameter vector $\boldsymbol{\theta}$ to the corresponding solution value of the i -th decision variable x_i returned by the solution algorithm h . For notational convenience, we denote $g(\boldsymbol{\theta}) = (g_f(\boldsymbol{\theta}), g_{\mathbf{x}}(\boldsymbol{\theta}))$.

The main goal of this work is to generate explanations that are coherent regarding the structure of the underlying optimization problem (2). More precisely, we say the model g is *coherent* for instance $\boldsymbol{\theta}$ if

$$f(g_{\mathbf{x}}(\boldsymbol{\theta}); \boldsymbol{\theta}) = g_f(\boldsymbol{\theta}), \quad (3)$$

$$g_{\mathbf{x}}(\boldsymbol{\theta}) \in \mathbb{X}(\boldsymbol{\theta}). \quad (4)$$

That is, the predictions are aligned with the underlying problem structure. Condition (3) ensures that the predictions for the decision variables \mathbf{x} , when applied to f , lead to the same objective value as the corresponding prediction for the objective value itself. Condition (4) ensures that the predictions of the decision variables are feasible for the corresponding problem.

To find an explanation, we first generate a training data set \mathcal{D} by sampling vectors $\boldsymbol{\theta}^i \in \Theta$, $i \in [N]_1$ which are close to $\boldsymbol{\theta}^0$. For each problem $i \in [N]_0$, we apply algorithm h which returns $h(\boldsymbol{\theta}^i) = (f(\mathbf{x}^i; \boldsymbol{\theta}^i), \mathbf{x}^i)$ consisting of a feasible solution \mathbf{x}^i and the corresponding objective function value $f(\mathbf{x}^i, \boldsymbol{\theta}^i)$. We aim for local fidelity, *i.e.*, we want to find models locally faithful to the optimization model such that $g_f(\boldsymbol{\theta}^i) \approx f(\mathbf{x}^i; \boldsymbol{\theta}^i)$ and $g_{\mathbf{x}}(\boldsymbol{\theta}^i) \approx \mathbf{x}^i$ for all $i \in [N]_0$.

Generating Explanations with LIME. In principle, LIME as in Eq. (1) can be applied to any black box function, hence it can be used to explain our solution algorithm h . To this end, all explainable predictors in g are fitted by solving the following problem

$$\arg \min_{g \in \mathcal{G}^{p+1}} \sum_{i=0}^N w^i (\ell_F(g(\boldsymbol{\theta}^i), h(\boldsymbol{\theta}^i)) + \Omega(g)), \quad (5)$$

where $\mathcal{G}^{p+1} = \mathcal{G} \times \dots \times \mathcal{G}$ and \mathcal{G} is the set of explainable functions, *e.g.*, linear functions, the scalars $w^i \geq 0$ denote the sample weights, ℓ_F denotes the fidelity loss, and Ω is a complexity measure. The corresponding functions g_f and $g_{\mathbf{x}}$ provide explainable predictors for components of the model; *i.e.*, objective value and decision variables. However, this model does not account for the coherence of the calculated predictors with the underlying structure of problem (2). As our experiments in Section 4 show, indeed the corresponding predictors in g are usually not coherent, *i.e.*, they violate Conditions (3) and (4) significantly. We use the latter approach as a benchmark method.

Coherent Explanations with CLEMO. To generate coherent explanations we solve the problem

$$\arg \min_{g \in \mathcal{G}^{p+1}} \sum_{i=0}^N w^i (\ell_F(g(\boldsymbol{\theta}^i), h(\boldsymbol{\theta}^i)) + R_C(g(\boldsymbol{\theta}^i))), \quad (6)$$

where $\mathcal{G}^{p+1} = \mathcal{G} \times \dots \times \mathcal{G}$ and \mathcal{G} is the set of interpretable functions, the scalars $w^i \geq 0$ denote the sample weights, ℓ_F denotes the fidelity loss, and R_C corresponds to the coherence regularizer that punishes predictors which do not admit the coherence conditions (3) and (4).

We note that theoretically, the coherence conditions could be added as constraints to the minimization problem (5). However, there is no guarantee that a feasible solution g exists, hence we enforce coherence via a regularizer. Similar to LIME, a complexity measure Ω could be added to the loss function if, for example, linear models with sparse weights are desired. We omit this term for ease of notation and to investigate the trade-off between fidelity and coherence. Note that ℓ_F and R_C can contain hyperparameters to balance all components of the loss function.

In principle, any appropriate function can be used for the fidelity and the coherence regularizer. We propose to use the squared loss

$$\ell_F(g(\boldsymbol{\theta}^i), h(\boldsymbol{\theta}^i)) = \|g(\boldsymbol{\theta}^i) - h(\boldsymbol{\theta}^i)\|^2 \quad (7)$$

as fidelity loss, and for the coherence regularizer, we use

$$R_C(g(\boldsymbol{\theta}^i)) = \lambda_{C_1} (g_f(\boldsymbol{\theta}^i) - f(g_{\mathbf{x}}(\boldsymbol{\theta}^i); \boldsymbol{\theta}^i))^2 + \lambda_{C_2} \delta(g_{\mathbf{x}}(\boldsymbol{\theta}^i), \mathbb{X}(\boldsymbol{\theta}^i)), \quad (8)$$

where $\delta(\mathbf{x}, \mathbb{X}(\boldsymbol{\theta}))$ denotes a distance measure between a point \mathbf{x} and the feasible set $\mathbb{X}(\boldsymbol{\theta})$. The values $\lambda_{C_1}, \lambda_{C_2}$ are hyperparameters to balance the losses. The R_C -regularizer measures incoherence, the first term punishes the violation of the coherence condition (3), while the second term punishes the violation of the coherence condition (4). Note that a mathematical formulation of the optimization problem is needed to formulate R_C . However, independent of the solution algorithm h , any valid formulation can be used as long as it contains all decisions x_i that have to be explained. Given a formulation, a natural choice for the distance measure is the sum of constraint violations of a solution. For example, if the feasible region is given by a set of constraints $\mathbb{X}(\boldsymbol{\theta}^i) = \{\mathbf{x} : \gamma_t(\mathbf{x}, \boldsymbol{\theta}^i) \leq 0, t = 1, \dots, T\}$, then we define

$$\delta(\mathbf{x}, \mathbb{X}(\boldsymbol{\theta}^i)) = \sum_{t=1}^T \max\{0, \gamma_t(\mathbf{x}, \boldsymbol{\theta}^i)\}. \quad (9)$$

While problem (6) can be applied to different classes of hypothesis sets \mathcal{G} , we restrict \mathcal{G} to linear models in this work. In this case we have coefficient vectors $\boldsymbol{\beta}_f, \boldsymbol{\beta}_{x_1}, \dots, \boldsymbol{\beta}_{x_p}$, such that $g_f(\boldsymbol{\theta}^i; \boldsymbol{\beta}) := \boldsymbol{\beta}_f^\top \boldsymbol{\theta}^i$ and $g_x(\boldsymbol{\theta}^i; \boldsymbol{\beta}) := (\boldsymbol{\beta}_{x_1}^\top \boldsymbol{\theta}^i, \dots, \boldsymbol{\beta}_{x_p}^\top \boldsymbol{\theta}^i)$. Using this parametrization we can formalize the explanation by the matrix $\boldsymbol{\beta} \equiv (\boldsymbol{\beta}_f, \boldsymbol{\beta}_{x_1}, \dots, \boldsymbol{\beta}_{x_p})^\top \in \mathbb{R}^{(p+1) \times q}$ such that each row corresponds to a linear explanation model for a component of the optimization model. Problem (6) then becomes

$$\arg \min_{\boldsymbol{\beta}} \sum_{i=0}^N w^i (\ell_F(\boldsymbol{\beta}^\top \boldsymbol{\theta}^i, h(\boldsymbol{\theta}^i)) + R_C(\boldsymbol{\beta}^\top \boldsymbol{\theta}^i)). \quad (10)$$

Note that CLEMO can easily be adjusted if only a subset of components has to be explained. In this case, we replace $g_c(\boldsymbol{\theta}^i; \boldsymbol{\beta})$ by the true value $h_c(\boldsymbol{\theta}^i)$ in the above model for all components $c \in \{f, x_1, \dots, x_p\}$ which do not have to be explained. This is especially useful if optimization problem (2) contains a large number of decision variables, or variables that do not need to be explained, like auxiliary variables (e.g., slack variables) or variables for which the value does not vary.

Since we use the squared loss, Eq. (7), in problem (10), the first term corresponding to the fidelity loss becomes a convex function of $\boldsymbol{\beta}$. For the coherence regularizer, the following holds.

Proposition 3.1. *Suppose that $g(\boldsymbol{\theta}) = \boldsymbol{\beta}^\top \boldsymbol{\theta}$ in Eq. (8). If the following conditions hold, then the coherence regularizer term in (10) is a convex function of $\boldsymbol{\beta}$:*

- (1) *The function $\mathbf{x} \mapsto f(\mathbf{x}; \boldsymbol{\theta})$ is affine.* (2) *The function $\mathbf{x} \mapsto \delta(\mathbf{x}, \mathbb{X}(\boldsymbol{\theta}))$ is convex.*

The proof of this proposition follows from applying the composition rules of convex functions (Boyd & Vandenberghe, 2004). When the conditions in this proposition are satisfied, every local minimum of problem (10) is a global minimum. We can use first-order methods to find such a minimum if the functions are differentiable. We note that for δ as defined in Eq. (9), we have that Eq. (8) is convex in $\boldsymbol{\beta}$ if the functions $\mathbf{x} \mapsto \gamma_t(\mathbf{x}, \boldsymbol{\theta}^i)$ are convex in \mathbf{x} for $t \in [T]_1$ since $x \mapsto \max\{0, x\}$ is convex and nondecreasing in x . Assuming that $\boldsymbol{\beta}$ comes from a bounded space, we can then use the subgradient algorithm with constant step size and step length and ensure convergence to an ϵ -optimal point within a finite number of steps in $\mathcal{O}(1/\epsilon^2)$ (Boyd et al., 2003).

Weights. We define the weights (similarly to LIME) as the radial basis function kernel with kernel parameter ν and distance function d ,

$$w^i = \exp(-d(\boldsymbol{\theta}^i, \boldsymbol{\theta}^0)^2 / \nu^2), \quad i \in [N]_0. \quad (11)$$

Sampling. We recall that contrary to ML models, optimization models do not require model training per se. Therefore, $\boldsymbol{\theta}^i$ cannot be sampled according to the train data distribution. Depending on the context, $\boldsymbol{\theta}^i$ can be sampled from relevant distributions, e.g., historic data, or with pre-determined rules, e.g., discretization. Besides, we note that optimization problem can have immutable parameters, so for some values of $\boldsymbol{\theta}^i$ might yield infeasible or unbounded instances. Therefore, sampling requires domain knowledge on which parameters are mutable and hence relevant for an explanation. We ensure the generated dataset \mathcal{D} contains only feasible, bounded instances of the optimization problem.

Binary Decision Variables. We opt for logistic regression to obtain interpretable surrogate models for the output components of the optimization problem that are restricted to binary values. Let $\mathcal{B} \subseteq \{f, x_1, \dots, x_p\}$ be the set of binary components. Then, for a binary component $c \in \mathcal{B}$, we consider predictors of the form $g_c(\boldsymbol{\theta}) = \sigma(\boldsymbol{\beta}_c^\top \boldsymbol{\theta})$ with $\sigma : \mathbb{R} \rightarrow [0, 1]$ the sigmoid function. The relative values of vector $\boldsymbol{\beta}_c$ then tell the user the feature importance for the probability of the

Algorithm 1 CLEMO

Input: Optimization problem with parameter θ^0 , solution algorithm h , family of functions \mathcal{G}
 $\theta^i \leftarrow \text{sample_around}(\theta^0)$ for $i \in [N]_1$
 $(f(x^i; \theta^i), x^i) \leftarrow h$ applied to Eq. (2) with θ^i for $i \in [N]_0$
 $w^i \leftarrow$ weight function Eq. (11) for $i \in [N]_0$
 $\mathcal{D} \leftarrow \{(\theta^i, (f(x^i; \theta^i), x^i)) : i \in [N]_0\}$
 $g^* \leftarrow$ solution of Problem Eq. (6) over \mathcal{G}
Return: Explainable function g^*

component being 0 or 1. For the binary components, we measure the fidelity using the log-loss. The total fidelity loss then becomes

$$\lambda_{F_1} \sum_{c \in \bar{\mathcal{B}}} \|\beta_c^\top \theta^i - h_c(\theta^i)\|^2 - \lambda_{F_2} \sum_{c \in \mathcal{B}} h_c(\theta^i) \ln(\sigma(\beta_c^\top \theta^i)) + (1 - h_c(\theta^i)) \ln(1 - \sigma(\beta_c^\top \theta^i)),$$

where $\bar{\mathcal{B}} = \{f, x_1, \dots, x_p\} \setminus \mathcal{B}$ and $\lambda_{F_1}, \lambda_{F_2} \geq 0$ are hyperparameters to balance the different losses.

The whole procedure of CLEMO is shown in Algorithm 1. For more details regarding the substeps we refer to Algorithms 2 and 3 in the appendix.

Guaranteed Objective Coherence in the Linear Case. Assume our present problem (2) has a linear objective function, *i.e.*, the objective is of the form $f(x; \theta) = \hat{c}^\top x$, and assume that only the feasible region is sensitive, *i.e.*, \hat{c} remains fixed. In this case, we can fit $p + 1$ independent linear models for each component in $c \in \{f, x_1, \dots, x_p\}$ by solving the classical weighted mean-square problem

$$\min_{\beta_c} \sum_{i=0}^N w^i \|\beta_c^\top \theta^i - h_c(\theta^i)\|^2.$$

If the minimizers are unique, the corresponding linear predictors provably fulfill the coherence condition (3), *i.e.*, in this case we do not need to apply the regularizer R_C to achieve coherence condition (3). However, it may happen that condition (4) is violated as the example from the introduction shows. A proof of the latter coherence statement can be found in Appendix A.3 (Theorem A.1).

4 EXPERIMENTS

In this section, we present three experiments. Each experiment considers a distinct optimization model and solver. The first experiment is used as a proof of concept, where we will show that CLEMO approximates the optimal decision and objective value function well for an instance of the Shortest Path Problem (SPP) with a single sensitive parameter. Next, in an extensive study, we consider exact solutions of various instances of the Knapsack Problem (KP). We compare the quality of explanations found by CLEMO to benchmarks by analyzing local fidelity, coherence, and stability of the found explanations when subjected to resampling. Lastly, we generate explanations for the Google OR-Tools heuristic (Furnon & Perron) applied to an instance of the Capacitated Vehicle Routing Problem (CVRP). The code of our experiments can be found at <https://anonymous.4open.science/r/CLEMO-899F>. All experiments are done on a computer with a 13th Gen Intel(R) Core(TM) i7-1355U 1.70 GHz processor and 64 GB of installed RAM.

Setup. Unless stated otherwise, all upcoming experiments use the following setup. Given an optimization problem for a given parameter vector θ^0 , we create a training data set \mathcal{D} of size 1000 by sampling $\theta^i \sim \mathcal{N}(\theta^0, 0.2\theta^0)$. The sample’s proximity weights w^i are determined using Eq. (11) with Euclidean distance and parameter ν equal to the mean distance to θ^0 over the data set \mathcal{D} .

As a benchmark for CLEMO, we consider generating explanations with the LIME-type method described in Section 3. We solve problem (5) where we fit logistic regression models for all binary output components and linear models for all other output components without any complexity regularization. We refer to this benchmark as LR.

For CLEMO we use the loss function stated in Eq. (10), where ℓ_F is given as in Eq. (12) and R_C is given as in Eq. (8) with δ defined as in Eq. (9). This way we can quantitatively compare CLEMO to

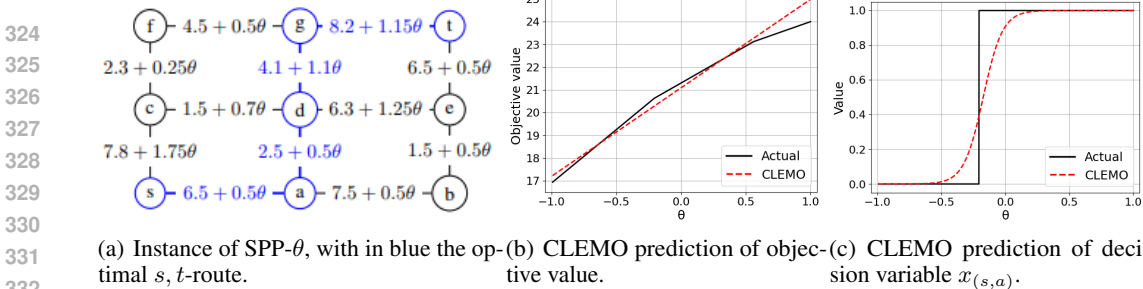


Figure 1: Solution of shortest path of SPP- θ instance as determined by Dijkstra’s Algorithm and as predicted by CLEMO.

the benchmark on local fidelity Eq. (12) and incoherence Eq. (8). In CLEMO, each term of the total loss function is weighted with hyperparameters $\lambda_{F_1}, \lambda_{F_2}, \lambda_{C_1}$, and λ_{C_2} as

$$\lambda_{F_1} \ell_{F_1}(g(\theta^i), h(\theta^i)) + \lambda_{F_2} \ell_{F_2}(g(\theta^i), h(\theta^i)) + \lambda_{C_1} R_{C_1}(g(\theta^i)) + \lambda_{C_2} R_{C_2}(g(\theta^i)).$$

To determine the hyperparameters, we calculate the weights using the LR benchmark solution to ensure that each loss term contributes to the total loss with similar order of magnitude. To this end, let \mathcal{L}_j be the value of loss term j for $j \in \{F_1, F_2, C_1, C_2\}$ when the LR benchmark solution is evaluated, and let \mathcal{L}_{\max} denote the largest of the four loss terms. For our experiments, we set $\lambda_j = 1$ when $\mathcal{L}_j = \mathcal{L}_{\max}$ or when $\mathcal{L}_j = 0$, and set $\lambda_j = 0.5\mathcal{L}_{\max}/\mathcal{L}_j$ otherwise. We solve problem (10) using the SLSQP solver of the `scipy` package. We set a maximum of 1000 iterations and warm-start the method with the LR benchmark solution. In Table 5 in the Appendix, we show in an ablation study why both regularizers R_{C_1} and R_{C_2} are needed to gain improvements in both coherence conditions (3) and (4). Moreover, in Tables 6 and 7 in the appendix, we compare different initializations and optimization methods, indicating that our setup below is the best choice in terms of runtime and solution quality.

4.1 SHORTEST PATH PROBLEM

As a first experiment, we explain an instance of the Shortest Path where possible cost-changes depend on a single parameter. An instance of the SPP is given by a connected graph $G = (V, E, c)$, with nodes V , edges E and edge-costs c , and specified start and terminal nodes $s, t \in V$. The objective is to find a path between s and t of minimum cost. Several methods exist for solving the SPP in polynomial time (Gallo & Pallottino, 1988). Here, we use Dijkstra’s algorithm.

We study the parametric version of the shortest path problem (SPP- θ), denoted by $G = (V, E, c + \theta\tilde{c})$. The edge costs are parametrized by the value θ and are given as the original edge costs (c) plus θ times a perturbation cost vector (\tilde{c}). The decision variables are denoted by x_{jk} and equal 1, if edge (v_j, v_k) is used in the solution and 0, otherwise. The parametrized SPP is then given as $\min\{(c + \theta\tilde{c})^T x : x \in \mathbb{X}_{SPP}\}$, where \mathbb{X}_{SPP} denotes the set of incidence vectors of all paths in the graph. The full formulation can be found in Eq. (12) in the appendix. We examine how the objective value and decision variable values of the original instance are affected by parameter θ . We consider the instance of SPP- θ as displayed in Fig. 1(a) with $\theta^0 = 0$ as the present problem. By varying θ , the optimal shortest (s, t) -path and its optimal value changes.

We sample θ uniformly on the interval $[-1, 1]$ and run CLEMO on the sampled data. In Fig. 1(b), we show the true dependency of the optimal value of SPP- θ and θ and the prediction of CLEMO. Fig. 1(c) shows the same for the dependency of three selected decision variable values. For the predictions of all decision variables, see Fig. 4 in the appendix. Both results show that CLEMO manages to be locally faithful. In Table 1, we show the fidelity and the incoherence of CLEMO and the LR benchmark. We can conclude that our method finds significantly more coherent explanations without considerably conceding fidelity.

Table 1: Weighted fidelity loss and incoherence of explaining Dijkstra’s algorithm applied to SPP- θ using the LR benchmark and using CLEMO.

	Infidelity (ℓ_F)		Incoherence (R_C)	
	Objective value	Decision vector	Objective	Feasible region
LR	32.03	648.06	112.52	54.55
CLEMO	32.12	646.28	6.91	21.08

Table 2: Mean (μ) and standard deviation (σ) of weighted fidelity loss and incoherence for the KP solved optimally. On the right, the mean stability measures over 10 instances per type of KP.

Method	Infidelity (ℓ_F)		Incoherence (R_C)				Stability			
	μ	σ	μ	σ	μ	σ	Std.	Normalized Std.	FSI	
Type 1	DTR	405	97.4	6.48	2.55	22.50	4.99	0.18	5.36	2.02
	LR	437	140	0.24	0.15	5.49	1.51	0.22	1.70	2.44
	CLEMO	479	157	0.08	0.06	0.01	0.004	0.18	1.75	2.26
Type 2	DTR	868	67.4	20.09	2.27	38.55	2.03	0.14	2.74	3.00
	LR	1076	99.4	1.01	0.12	9.49	0.68	0.19	0.74	3.40
	CLEMO	1203	113	0.38	0.06	0.03	0.01	0.16	0.81	3.34
Type 3	DTR	865	66.8	28.45	3.36	39.41	2.02	0.14	2.77	2.91
	LR	1061	97.8	1.39	0.16	9.90	0.64	0.20	0.71	3.22
	CLEMO	1189	113	0.58	0.07	0.04	0.01	0.16	0.79	3.23
Type 4	DTR	893	56.5	13.80	2.16	37.74	2.35	0.14	2.52	2.99
	LR	1111	77.6	0.70	0.11	8.94	0.74	0.18	0.66	3.31
	CLEMO	1241	87.56	0.27	0.06	0.03	0.01	0.16	0.77	3.38

Table 3: Runtime of different explanation approaches for various sizes of KP.

#items	KP #features	Runtime (s)		
		DTR	LR	CLEMO
5	10	0.0189	0.0031	8.54
10	20	0.0396	0.0790	50.0
20	40	0.183	0.0830	413
40	80	0.683	0.316	> 1000

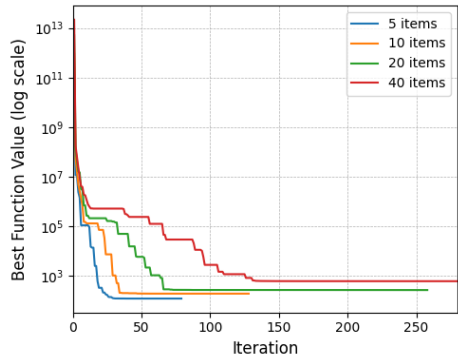


Figure 2: Convergence of CLEMO over SLSQP iterations for different sizes of KP.

4.2 KNAPSACK PROBLEM

Next, we present an extensive study on the Knapsack problem (KP). In this problem, we are given a set of items each with a corresponding value v_j and weight w_j . The goal is to decide how much of each item should be chosen to maximize the total value while not exceeding the capacity, which *w.l.o.g.* we set to 1. Formulated as a linear problem this becomes $\max\{v^\top x : w^\top x \leq 1, x \in [0, 1]^p\}$. We consider the parametrized KP, by setting $\theta = (v, w)$ and use Gurobi (Gurobi Optimization, LLC, 2024) to solve to optimality. This experiment compares CLEMO with two benchmark explanation methods: independently fitting the components using (i) a linear regression model (LR), and (ii) a decision tree regressor (DTR) with a maximum depth of 5, and minimum samples per leaf of 50. Here, we consider 40 instances of the KP each with $p = 25$ items. The 40 instances are divided over four instance types as described by (Pisinger, 2005): 1) uncorrelated, 2) weakly correlated, 3) strongly correlated, 4) inversely strongly correlated.

In Table 2, we see that compared to a linear regression approach the linear model found by CLEMO reduces the weighted incoherence in the objective and the constraint by more than 50% and 99% respectively, while the weighted fidelity loss increased only by roughly 20%. In Figs. 5 to 8 in the appendix, we plotted the fidelity loss and incoherence of each instance to strengthen our conclusion.

Besides, as datasets are randomly generated, we measure the stability of explanations over resampling. For the KP, we analyze the stability of CLEMO by using 10 different randomly generated datasets, resulting in 10 surrogate models. To quantify stability we use the (normalized) standard deviation of the feature contributions of g which is also used to examine the stability of LIME (Shankaranarayana & Runje, 2019). In Table 2, we consider the (normalized) standard deviation of the contribution of the top-5 most contributing, nonzero features for each component of $h(\theta)$. Besides, we examine the feature stability index (FSI), which is based on the variables stability index as presented in Visani et al. (2022). The FSI measures how much the order in feature contribution over the resamples on average coincides. Here, it takes values between 0 and 5, where a higher FSI indicates more stable explanations. An extensive description of the FSI can be found in Appendix A.5.2 in the appendix. From Table 2, we can conclude that the stability of CLEMO is comparable to the benchmark approaches.

Table 4: Weighted fidelity loss and incoherence of explaining Google OR-Tools applied to the CVRP instance using the LR benchmark and using CLEMO.

	Infidelity (ℓ_F)		Incoherence (R_C)	
	Objective value	Decision vector	Objective	Feasible region
LR	4.24	1207	12.35	802.55
CLEMO	4.24	1198	11.77	780.26

Runtime. To compare the runtime of CLEMO to benchmark methods, we analyze the runtime on Knapsack problems with 5, 10, 20, and 40 items. In Table 3, we see CLEMO takes longer to find an explanation. Looking at Fig. 2, we observe that CLEMO efficiently converges to a solution. Hence, early stopping could reduce runtimes while still ensuring more coherent explanations.

4.3 VEHICLE ROUTING PROBLEM

An instance of CVRP is given by a complete graph $G = (V, A)$, where V consists of a depot node v_0 and n client nodes each with a corresponding demand d_j . Moreover, each arc (v_j, v_k) has associated costs c_{jk} . Lastly, there are m vehicles, each with a capacity of M . The goal of the problem is to find at most m routes of minimum costs such that each route starts and ends at the depot, each client is visited exactly once, and the total demand on each route does not exceed the vehicle capacity. To formulate R_C , we use the Miller-Tucker-Zemlin formulation for the CVRP, which can be found in Eq. (13) in the appendix. The decision variables are then denoted by x_{jk} and equal 1 if arc (v_j, v_k) is used in the solution, and 0, otherwise. For this experiment, we consider the parameter vector consisting of the demands d and the costs of the arcs from the clients to the depot c_0 , i.e., $\theta = (d, c_0)$. The present problem has symmetric costs and consists of 16 clients and 4 vehicles. As a solver for this NP-hard problem, we let the Google OR-Tools heuristic search for a solution for 5 seconds (Furnon & Perron). We aim for explanations for the objective value, and which clients are visited before returning to the depot, i.e., the decision variables x_{j0} for $j \in [n]_1$.

As shown in Table 4, the explanation found by CLEMO is significantly more coherent without a considerable loss in fidelity compared to the LR benchmark. We visualize the explanations found by CLEMO in Fig. 3, where we first see the solution to the present problem found by Google OR-Tools in gray. Next, the feature contribution of the demands and costs are visualized via node and edge colors respectively. Combined with an overview of the top 10 most contributing features, this shows which features are the key components influencing the objective value as found by the solver. Thus, Fig. 3 tells us that the objective value is mainly affected by the distance towards the nodes far from the depot. In Fig. 9 in the appendix, we present an additional explanation for the decision variable x_{20} .

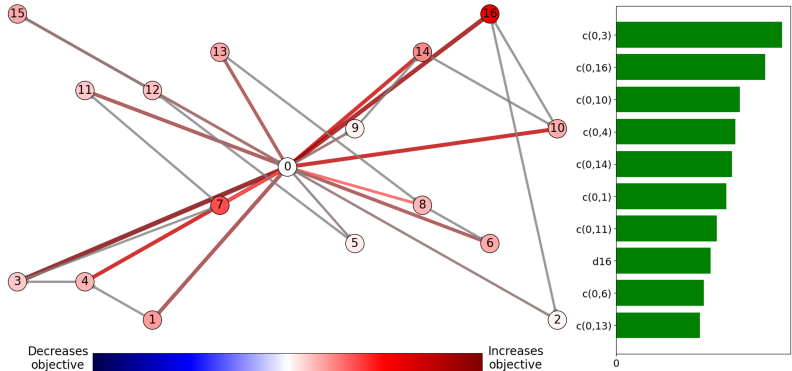


Figure 3: Explanation as found by CLEMO for the objective value visualized in the present problem network structure. Also, the top 10 relative feature contributions is depicted on the right.

5 CONCLUSION & LIMITATIONS

In this paper, we propose CLEMO, a sampling-based method that can be used to explain arbitrary exact or heuristic solution algorithms for optimization problems. Our method provides local explanations for the objective value and decision variables of mathematical optimization models. Contrary to existing methods, CLEMO enforces explanations that are coherent with the underlying model structure which enhances transparent decision-making. By applying CLEMO to various optimization

486 problems we have shown that we can find explanations that are significantly more coherent than
487 benchmark explanations generated using LIME without substantially compromising fidelity. At the
488 same time, including coherence losses to CLEMO leads to longer runtimes. To manage the increase
489 the runtime, an early stopping criterion could be implemented in the gradient descent procedure
490 when minimizing the total loss function. Another option is to reduce the input space by performing
491 discretization or by a mechanism that selects a sparse set of features. Lastly, one could opt to explain
492 parts of the solution, *e.g.*, explaining the objective value and a subset of decision variables.

493 Where CLEMO is a model-agnostic explanation method, it requires some domain knowledge.
494 Contrary to ML models, there is not necessarily historical or training data available upon which to
495 base a sampling mechanism. In this case, to ensure feasible and bounded instances, we need to know
496 which parameters are mutable. Likewise, setting up the coherence regularizer relies on the available
497 information about the problem formulation. In many cases this information is known. However,
498 when only part of the constraints is known, *e.g.*, if a black-box solver incorporates additional internal
499 constraints, CLEMO could still use known information to derive the coherence regularizers.

500 This work focuses on explaining the objective value and decision variables. However, one could
501 easily extend the concept to explanations of other components, such as constraint slacks, runtime,
502 optimality gap, etc. For now, CLEMO uses parametric regression models for explanations. Another
503 extension of our work could be to consider other types of interpretable functions, such as decision
504 trees. Lastly, CLEMO could be a useful method to explain synergies between ML and optimization
505 models, *e.g.*, in predict-then-optimize models.
506
507
508
509
510
511
512
513
514
515
516
517
518
519
520
521
522
523
524
525
526
527
528
529
530
531
532
533
534
535
536
537
538
539

REFERENCES

- 540
541
542 Amina Adadi and Mohammed Berrada. Peeking Inside the Black-Box: A Survey on Explain-
543 able Artificial Intelligence (XAI). *IEEE Access*, 6:52138–52160, 2018. ISSN 2169-3536. doi:
544 10.1109/ACCESS.2018.2870052. URL [https://ieeexplore.ieee.org/document/
545 8466590/?arnumber=8466590](https://ieeexplore.ieee.org/document/8466590/?arnumber=8466590). Conference Name: IEEE Access.
- 546 Kevin-Martin Aigner, Marc Goerigk, Michael Hartisch, Frauke Liers, and Arthur Miehlich. A
547 Framework for Data-Driven Explainability in Mathematical Optimization. *Proceedings of the AAAI
548 Conference on Artificial Intelligence*, 38(19):20912–20920, March 2024. ISSN 2374-3468. doi: 10.
549 1609/aaai.v38i19.30081. URL [https://ojs.aaai.org/index.php/AAAI/article/
550 view/30081](https://ojs.aaai.org/index.php/AAAI/article/view/30081). Number: 19.
- 551 Yoshua Bengio, Andrea Lodi, and Antoine Prouvost. Machine learning for combinatorial optimization:
552 a methodological tour d’horizon. *European Journal of Operational Research*, 290(2):405–421,
553 2021.
- 554 Dimitris Bertsimas and John N Tsitsiklis. *Introduction to Linear Optimization*, volume 6. Athena
555 scientific Belmont, MA, 1997.
- 556 Francesco Bodria, Fosca Giannotti, Riccardo Guidotti, Francesca Naretto, Dino Pedreschi, and
557 Salvatore Rinzivillo. Benchmarking and survey of explanation methods for black box models. *Data
558 Mining and Knowledge Discovery*, 37(5):1719–1778, September 2023. ISSN 1573-756X. doi: 10.
559 1007/s10618-023-00933-9. URL <https://doi.org/10.1007/s10618-023-00933-9>.
- 560 Emanuele Borgonovo and Elmar Plischke. Sensitivity analysis: A review of recent advances.
561 *European Journal of Operational Research*, 248(3):869–887, February 2016. ISSN 0377-2217.
562 doi: 10.1016/j.ejor.2015.06.032. URL [https://www.sciencedirect.com/science/
563 article/pii/S0377221715005469](https://www.sciencedirect.com/science/article/pii/S0377221715005469).
- 564 Stephen Boyd and Lieven Vandenbergh. *Convex Optimization*. Cambridge University Press, 2004.
- 565 Stephen Boyd, Lin Xiao, and Almir Mutapcic. Subgradient methods. *lecture notes of EE392o,
566 Stanford University, Autumn Quarter, 2004(01)*, 2003.
- 567 Arun Das and Paul Rad. Opportunities and Challenges in Explainable Artificial Intelligence (XAI):
568 A Survey, June 2020. URL <http://arxiv.org/abs/2006.11371>. arXiv:2006.11371.
- 569 Jürgen Dieber and Sabrina Kirrane. Why model why? Assessing the strengths and limitations of
570 LIME, November 2020. URL <http://arxiv.org/abs/2012.00093>. arXiv:2012.00093
571 [cs].
- 572 Rudresh Dwivedi, Devam Dave, Het Naik, Smiiti Singhal, Rana Omer, Pankesh Patel, Bin Qian,
573 Zhenyu Wen, Tejal Shah, Graham Morgan, and Rajiv Ranjan. Explainable AI (XAI): Core
574 Ideas, Techniques, and Solutions. *ACM Computing Surveys*, 55(9):194:1–194:33, January 2023.
575 ISSN 0360-0300. doi: 10.1145/3561048. URL [https://dl.acm.org/doi/10.1145/
576 3561048](https://dl.acm.org/doi/10.1145/3561048).
- 577 Felix Engelhardt, Jannis Kurtz, Ş İlker Birbil, and Ted Ralphs. Counterfactual explanations for
578 integer optimization problems. *arXiv preprint arXiv:2510.17624*, 2025.
- 579 Alexandre Forel, Axel Parmentier, and Thibaut Vidal. Explainable Data-Driven Optimization: From
580 Context to Decision and Back Again. In *Proceedings of the 40th International Conference on
581 Machine Learning*, pp. 10170–10187. PMLR, July 2023. URL [https://proceedings.mlr.
582 press/v202/forel23a.html](https://proceedings.mlr.press/v202/forel23a.html). ISSN: 2640-3498.
- 583 Vincent Furnon and Laurent Perron. OR-Tools Routing Library. URL [https://developers.
584 google.com/optimization/routing/](https://developers.google.com/optimization/routing/).
- 585 Giorgio Gallo and Stefano Pallottino. Shortest path algorithms. *Annals of Operations Research*,
586 13(1):1–79, December 1988. ISSN 1572-9338. doi: 10.1007/BF02288320. URL <https://doi.org/10.1007/BF02288320>.
- 587
588
589
590
591
592
593

- 594 Marc Goerigk and Michael Hartisch. A framework for inherently interpretable optimization models.
595 *European Journal of Operational Research*, 310(3):1312–1324, November 2023. ISSN 0377-2217.
596 doi: 10.1016/j.ejor.2023.04.013. URL [https://www.sciencedirect.com/science/
597 article/pii/S0377221723002953](https://www.sciencedirect.com/science/article/pii/S0377221723002953).
- 598
599 Riccardo Guidotti. Counterfactual explanations and how to find them: literature review and
600 benchmarking. *Data Mining and Knowledge Discovery*, 38(5):2770–2824, September 2024.
601 ISSN 1573-756X. doi: 10.1007/s10618-022-00831-6. URL [https://doi.org/10.1007/
602 s10618-022-00831-6](https://doi.org/10.1007/s10618-022-00831-6).
- 603 Gurobi Optimization, LLC. Gurobi Optimizer Reference Manual, 2024. URL [https://www.
604 gurobi.com](https://www.gurobi.com).
- 605
606 Bertrand Iooss and Paul Lemaître. A review on global sensitivity analysis methods. *Uncertainty
607 management in simulation-optimization of complex systems: algorithms and applications*, pp.
608 101–122, 2015.
- 609
610 Imdat Kara, Gilbert Laporte, and Tolga Bektas. A note on the lifted Miller–Tucker–Zemlin
611 subtour elimination constraints for the capacitated vehicle routing problem. *European Jour-
612 nal of Operational Research*, 158(3):793–795, November 2004. ISSN 0377-2217. doi:
613 10.1016/S0377-2217(03)00377-1. URL [https://www.sciencedirect.com/science/
614 article/pii/S0377221703003771](https://www.sciencedirect.com/science/article/pii/S0377221703003771).
- 615
616 Anton Korikov and J. Christopher Beck. Objective-Based Counterfactual Explanations for Linear
617 Discrete Optimization. In Andre A. Cire (ed.), *Integration of Constraint Programming, Artificial
618 Intelligence, and Operations Research*, pp. 18–34, Cham, 2023. Springer Nature Switzerland.
619 ISBN 978-3-031-33271-5. doi: 10.1007/978-3-031-33271-5_2.
- 620
621 Anton Korikov, Alexander Shleyfman, and J. Christopher Beck. Counterfactual Explanations for
622 Optimization-Based Decisions in the Context of the GDPR. In *Proceedings of the Thirtieth Interna-
623 tional Joint Conference on Artificial Intelligence*, pp. 4097–4103, Montreal, Canada, August 2021.
624 International Joint Conferences on Artificial Intelligence Organization. ISBN 978-0-9992411-9-
625 6. doi: 10.24963/ijcai.2021/564. URL [https://www.ijcai.org/proceedings/2021/
626 564](https://www.ijcai.org/proceedings/2021/564).
- 627
628 Jannis Kurtz, Ş İlker Birbil, and Dick den Hertog. Counterfactual explanations for linear optimization.
629 *European Journal of Operational Research*, 2025.
- 630
631 Pantelis Linardatos, Vasilis Papastefanopoulos, and Sotiris Kotsiantis. Explainable AI: A Review
632 of Machine Learning Interpretability Methods. *Entropy*, 23(1):18, January 2021. ISSN 1099-
633 4300. doi: 10.3390/e23010018. URL <https://www.mdpi.com/1099-4300/23/1/18>.
634 Number: 1 Publisher: Multidisciplinary Digital Publishing Institute.
- 635
636 Scott M Lundberg and Su-In Lee. A unified approach to interpreting model predictions. *Advances in
637 neural information processing systems*, 30, 2017.
- 638
639 Dang Minh, H. Xiang Wang, Y. Fen Li, and Tan N. Nguyen. Explainable artificial intelli-
640 gence: a comprehensive review. *Artificial Intelligence Review*, 55(5):3503–3568, June 2022.
641 ISSN 1573-7462. doi: 10.1007/s10462-021-10088-y. URL [https://doi.org/10.1007/
642 s10462-021-10088-y](https://doi.org/10.1007/s10462-021-10088-y).
- 643
644 Jorge Nocedal and Stephen J. Wright. *Numerical Optimization*. Springer series in Operations
645 Research and Financial Engineering. Springer, New York, NY, 2. ed. edition, 2006.
- 646
647 Fotios Petropoulos, Gilbert Laporte, Emel Aktas, Sibel A Alumur, Claudia Archetti, Hayriye Ayhan,
648 Maria Battarra, Julia A Bennell, Jean-Marie Bourjolly, John E Boylan, et al. Operational Research:
649 methods and applications. *Journal of the Operational Research Society*, 75(3):423–617, 2024.
- 650
651 David Pisinger. Where are the hard knapsack problems? *Computers & Operations Research*, 32(9):
652 2271–2284, September 2005. ISSN 0305-0548. doi: 10.1016/j.cor.2004.03.002. URL <https://www.sciencedirect.com/science/article/pii/S030505480400036X>.

- 648 Saman Razavi, Anthony Jakeman, Andrea Saltelli, Clémentine Prieur, Bertrand Iooss, Emanuele
649 Borgonovo, Elmar Plischke, Samuele Lo Piano, Takuya Iwanaga, William Becker, Stefano
650 Tarantola, Joseph H. A. Guillaume, John Jakeman, Hoshin Gupta, Nicola Melillo, Giovanni
651 Rabitti, Vincent Chabridon, Qingyun Duan, Xifu Sun, Stefán Smith, Razi Sheikholeslami, Nasim
652 Hosseini, Masoud Asadzadeh, Arnald Puy, Sergei Kucherenko, and Holger R. Maier. The
653 Future of Sensitivity Analysis: An essential discipline for systems modeling and policy sup-
654 port. *Environmental Modelling & Software*, 137:104954, March 2021. ISSN 1364-8152. doi:
655 10.1016/j.envsoft.2020.104954. URL [https://www.sciencedirect.com/science/
656 article/pii/S1364815220310112](https://www.sciencedirect.com/science/article/pii/S1364815220310112).
- 657 Marco Tulio Ribeiro, Sameer Singh, and Carlos Guestrin. "Why Should I Trust You?": Explaining
658 the Predictions of Any Classifier. In *Proceedings of the 22nd ACM SIGKDD International
659 Conference on Knowledge Discovery and Data Mining*, pp. 1135–1144, San Francisco California
660 USA, August 2016. ACM. ISBN 978-1-4503-4232-2. doi: 10.1145/2939672.2939778. URL
661 <https://dl.acm.org/doi/10.1145/2939672.2939778>.
- 662 Sean Saito, Eugene Chua, Nicholas Capel, and Rocco Hu. Improving LIME Robustness with
663 Smarter Locality Sampling, March 2021. URL <http://arxiv.org/abs/2006.12302>.
664 arXiv:2006.12302 [cs, stat].
- 665 Lara Scavuzzo, Karen Aardal, Andrea Lodi, and Neil Yorke-Smith. Machine learning augmented
666 branch and bound for mixed integer linear programming. *Mathematical Programming*, pp. 1–44,
667 2024.
- 668
669 Sharath M Shankaranarayana and Davor Runje. Alime: Autoencoder based approach for local
670 interpretability. In *International conference on intelligent data engineering and automated learning*,
671 pp. 454–463. Springer, 2019.
- 672
673 Georg Still. Lectures on parametric optimization: An introduction. *Optimization Online*, pp. 2, 2018.
- 674
675 Giorgio Visani, Enrico Bagli, Federico Chesani, Alessandro Poluzzi, and Davide Capuzzo. Statistical
676 stability indices for LIME: obtaining reliable explanations for Machine Learning models. *Journal
677 of the Operational Research Society*, 73(1):91–101, January 2022. ISSN 0160-5682, 1476-9360.
678 doi: 10.1080/01605682.2020.1865846. URL <http://arxiv.org/abs/2001.11757>.
679 arXiv:2001.11757 [cs, stat].
- 680
681 Harvey M. Wagner. Global Sensitivity Analysis. *Operations Research*, 43(6):948–969, 1995. ISSN
0030-364X. URL <https://www.jstor.org/stable/171637>. Publisher: INFORMS.
- 682
683 Laurence A Wolsey. *Integer Programming*. John Wiley & Sons, 2020.
- 684
685 Muhammad Rehman Zafar and Naimul Khan. Deterministic Local Interpretable Model-Agnostic
686 Explanations for Stable Explainability. *Machine Learning and Knowledge Extraction*, 3(3):525–
687 541, September 2021. ISSN 2504-4990. doi: 10.3390/make3030027. URL [https://www.
688 mdpi.com/2504-4990/3/3/27](https://www.mdpi.com/2504-4990/3/3/27). Number: 3 Publisher: Multidisciplinary Digital Publishing
Institute.
- 689
690 Yujia Zhang, Kuangyan Song, Yiming Sun, Sarah Tan, and Madeleine Udell. "Why Should You
691 Trust My Explanation?" Understanding Uncertainty in LIME Explanations, June 2019. URL
<http://arxiv.org/abs/1904.12991>. arXiv:1904.12991.
- 692
693 Zhengze Zhou, Giles Hooker, and Fei Wang. S-LIME: Stabilized-LIME for Model Explanation. In
694 *Proceedings of the 27th ACM SIGKDD Conference on Knowledge Discovery & Data Mining*, pp.
695 2429–2438, Virtual Event Singapore, August 2021. ACM. ISBN 978-1-4503-8332-5. doi: 10.1145/
696 3447548.3467274. URL <https://dl.acm.org/doi/10.1145/3447548.3467274>.
- 697
698
699
700
701

A APPENDIX

A.1 MATHEMATICAL MODELS OF THE OPTIMIZATION PROBLEMS

In this section, we present the formulation of the Shortest Path problem Eq. (12) and the Capacitated Vehicle Routing problem Eq. (13). For the latter, we use the Miller-Tucker-Zemlin formulation as described in Kara et al. (2004).

Shortest Path Problem

$$\begin{aligned}
& \min (\mathbf{c} + \theta \hat{\mathbf{c}})^\top \mathbf{x} & (12) \\
& \text{s.t. } \sum_{(s,j) \in E} x_{s,j} - \sum_{(j,s) \in E} x_{j,s} = 1, \\
& \quad \sum_{(j,t) \in E} x_{j,t} - \sum_{(t,j) \in E} x_{t,j} = 1, \\
& \quad \sum_{(j,k) \in E} x_{j,k} - \sum_{(k,l) \in E} x_{k,l} = 0, & \forall k \neq s, t, \\
& \quad x_e \in \{0, 1\}, & \forall e \in E.
\end{aligned}$$

Capacitated Vehicle Routing Problem

$$\begin{aligned}
& \min \sum_{j=0}^n \sum_{k=0, k \neq j}^n c_{jk} x_{jk} & (13) \\
& \text{s.t. } \sum_{k=1}^n x_{1k} \leq m, \\
& \quad \sum_{j=1}^n x_{j1} \leq m, \\
& \quad \sum_{k=1}^n x_{1k} \geq 1, \\
& \quad \sum_{j=1}^n x_{j1} \geq 1, \\
& \quad \sum_{k=0, k \neq j}^n x_{jk} = 1, & j \in [n]_1, \\
& \quad \sum_{j=0, j \neq k}^n x_{jk} = 1, & k \in [n]_1, \\
& \quad u_j - u_j + M x_{jk} \leq M - d_k, & j, k \in [n]_1, \quad j \neq k \\
& \quad d_j \leq u_j \leq M, & j \in [n]_1, \\
& \quad x_{jk} \in \{0, 1\}, & j, k \in [n]_0, \quad j \neq k.
\end{aligned}$$

A.2 DETAILED ALGORITHM

Here, we present an extensive description of our explanation method CLEMO as used in the experiments. It consists of two parts, (i) creating a training dataset (Algorithm 2), and (ii) finding a surrogate model (Algorithm 3).

Algorithm 2 CLEMO - Creating a dataset

Input: Optimization problem with parameter θ^0 and solver algorithm h
Initialize samples = $\{\theta^0\}$, targets = $\{(f(\mathbf{x}^0; \theta^0), \mathbf{x}^0)\}$, weights = \emptyset , distances = $\{0\}$
while #samples < 1000 **do**
 $\theta^i \sim \mathcal{N}(\theta^0, 0.2\theta^0)$
 if Optimization model is feasible and bounded for θ^i **then**
 samples \leftarrow samples $\cup \{\theta^i\}$
 $(f(\mathbf{x}^i; \theta^i), \mathbf{x}^i) \leftarrow h$ applied to θ^i -problem
 targets \leftarrow targets $\cup \{(f(\mathbf{x}^i; \theta^i), \mathbf{x}^i)\}$
 distances \leftarrow distances $\cup \{\text{Euclidean distance}(\theta^0, \theta^i)\}$
 end if
end while
 $\bar{d} \leftarrow \text{average}(\text{distances})$
for θ^i in samples **do**
 weights \leftarrow weights $\cup \{\text{rbf}(\theta^0, \theta^i, \bar{d})\}$
end for
Return: $\mathcal{D} \leftarrow$ (samples, targets, weights)

Algorithm 3 CLEMO - Finding surrogate model

Input: Optimization problem, dataset \mathcal{D} , loss function consisting of components $\{\ell_{F_1}, \ell_{F_2}, R_{C_1}, R_{C_2}\}$
for output component $c \in \{f, x_1, \dots, x_p\}$ **do**
 if $h(\theta)_c$ is a binary value **then**
 $(\beta_{BM})_c \leftarrow \text{Logistic Regression fit}(\text{samples}, h(\theta)_c, \text{weights})$
 else
 $(\beta_{BM})_c \leftarrow \text{Linear Regression fit}(\text{samples}, h(\theta)_c, \text{weights})$
 end if
end for
 $\mathcal{L}_j \leftarrow \{\text{loss}_j(\beta_{BM}, \mathcal{D}) \mid \text{for } \text{loss}_j \in \{\ell_{F_1}, \ell_{F_2}, R_{C_1}, R_{C_2}\}\}$
 $\mathcal{L}_{\max} \leftarrow \text{maximum}(\mathcal{L}_{F_1}, \mathcal{L}_{F_2}, \mathcal{L}_{C_1}, \mathcal{L}_{C_2})$
for loss function component index j in $\{F_1, F_2, C_1, C_2\}$ **do**
 if $\mathcal{L}_j \in \{\mathcal{L}_{\max}, 0\}$ **then**
 $\lambda_j \leftarrow 1$
 else
 $\lambda_j \leftarrow 0.5\mathcal{L}_{\max}/\mathcal{L}_j$
 end if
end for
 $\text{total_loss_function} \leftarrow \lambda_{F_1}\ell_{F_1} + \lambda_{F_2}\ell_{F_2} + \lambda_{C_1}R_{C_1} + \lambda_{C_2}R_{C_2}$
 $\beta_{CL} \leftarrow \text{argmin}_{\beta} \text{total_loss_function}(\beta, \mathcal{D})$ using β_{BM} as a warm start
Return: Interpretable function β_{CL}

810 A.3 COHERENCE FOR LINEAR OPTIMIZATION PROBLEMS

811 In this section we prove the statement that independent fitting of linear predictors leads to objective
812 coherence under certain assumptions.

813 **Theorem A.1.** *The minimizers of the weighted least-square problems*

$$814 \min_{\beta_f} \sum_{i=0}^N w^i \|f(\mathbf{x}^i; \boldsymbol{\theta}^i) - \beta_f^\top \boldsymbol{\theta}^i\|^2$$

815 and

$$816 \min_{\beta_{x_j}} \sum_{i=0}^N w^i \|\mathbf{x}_j^i - \beta_{x_j}^\top \boldsymbol{\theta}^i\|^2 \quad j = 1, \dots, p$$

817 fulfill the coherence condition in Eq. (3).

818 *Proof.* Since the objective function $\hat{\mathbf{c}}^\top \mathbf{x}$ is fixed and linear we have

$$819 f(\mathbf{x}^i; \boldsymbol{\theta}^i) = \sum_{j=1}^p \hat{c}_j \mathbf{x}_j^i.$$

820 The weighted least-squares problem has the unique optimal solution

$$821 \beta_{x_j}^* = (\boldsymbol{\Theta}^\top \mathbf{W} \boldsymbol{\Theta})^+ \boldsymbol{\Theta}^\top \mathbf{W} \mathbf{y}^j \quad j = 1, \dots, p$$

822 and

$$823 \beta_f^* = (\boldsymbol{\Theta}^\top \mathbf{W} \boldsymbol{\Theta})^+ \boldsymbol{\Theta}^\top \mathbf{W} \mathbf{y}^f,$$

824 where $\boldsymbol{\Theta}$ is the matrix whose i -th row is the vector $\boldsymbol{\theta}^i$, \mathbf{W} is the matrix with weight w^i on the
825 diagonal and zeroes elsewhere, $(\boldsymbol{\Theta}^\top \mathbf{W} \boldsymbol{\Theta})^+$ is the pseudoinverse of $\boldsymbol{\Theta}^\top \mathbf{W} \boldsymbol{\Theta}$ \mathbf{y}^j is the vector where
826 the i -th entry is the value x_j^i and \mathbf{y}^f is the vector where the i -th entry is the value $f(\mathbf{x}^i; \boldsymbol{\theta}^i)$. We
827 assume here that $(\boldsymbol{\Theta}^\top \mathbf{W} \boldsymbol{\Theta})$ is invertible. Then for any new parameter vector $\boldsymbol{\theta}$ the predicted optimal
828 value of our model is

$$829 \begin{aligned} 830 \boldsymbol{\theta}^\top \beta_f &= \boldsymbol{\theta}^\top (\boldsymbol{\Theta}^\top \mathbf{W} \boldsymbol{\Theta})^+ \boldsymbol{\Theta}^\top \mathbf{W} \mathbf{y}^f \\ 831 &= \boldsymbol{\theta}^\top (\boldsymbol{\Theta}^\top \mathbf{W} \boldsymbol{\Theta})^+ \boldsymbol{\Theta}^\top \mathbf{W} \left(\sum_{j=1}^p \hat{c}_j \mathbf{y}^j \right) \\ 832 &= \sum_{j=1}^p \hat{c}_j \boldsymbol{\theta}^\top (\boldsymbol{\Theta}^\top \mathbf{W} \boldsymbol{\Theta})^+ \boldsymbol{\Theta}^\top \mathbf{W} \mathbf{y}^j \\ 833 &= \sum_{j=1}^p \hat{c}_j \boldsymbol{\theta}^\top \beta_{x_j}, \end{aligned}$$

834 which means that the predictors are coherent regarding condition Eq. (3). □

A.4 MODELING CHOICES

Ablation study We checked the effect of the regularizer on the solution by performing an ablation study on a Knapsack problem with 5 items. The results in Table 5 show that each regularizer contributes to reducing the incoherence. When CLEMO considers fidelity as well as both coherence regularizers, we see an improvement in both coherent conditions (3) and (4), while marginally giving in on fidelity. Note that the first row corresponds to the benchmark method, while the last row represents the λ values used by CLEMO in the experiments in this work.

Table 5: Ablation study for a Knapsack instance with 5 items

λ_F	λ_{C_1}	λ_{C_2}	Infidelity (ℓ_f)	Incoherence (R_C)	
				Objective	Constraints
1	0	0	95.58	0.32	4.61
0	148.1	0	1102.02	$3.51 \cdot 10^{-9}$	276.65
0	0	10.4	10452.98	5015.66	0.00
1	148.1	0	103.29	0.094	13.11
1	0	10.4	96.74	0.98	0.022
0	148.1	10.4	3284.81	$1.02 \cdot 10^{-6}$	0.00
1	148.1	10.4	104.43	0.12	0.044

Iterative methods We compared runtimes of different iterative methods within the SciPy minimize package for a Knapsack problem with 5 items. The results show that the runtime of our chosen iterative method, *SLSQP*, is in the same order of magnitude as the most efficient iterative methods we checked.

Table 6: Total training Loss and time to completion for various iterative methods available for SciPy.

Method	Time to completion	Training Loss
COBYLA	7.52E+00 seconds	1.38E+02
<i>SLSQP</i>	<i>9.63E+00 seconds</i>	1.23E+02
Nelder-Mead	1.10E+01 seconds	1.36E+02
BFGS	4.35E+01 seconds	1.23E+02
COBYQA	5.03E+01 seconds	1.35E+02
TNC	7.53E+01 seconds	1.23E+02
L-BFGS-B	8.38E+01 seconds	1.23E+02
trust-constr	1.01E+02 seconds	1.23E+02
CG	2.16E+02 seconds	1.24E+02
Powell	3.64E+02 seconds	1.25E+02
Newton-CG	7.71E+02 seconds	1.24E+02

Initialization of solution For the Shortest Path problem, we additionally ran CLEMO with (i) 0 initialization, (ii) 1 initialization, and (iii) 10 randomly generated initializations ($\mathcal{U}[-10, 10]$). Note that due to the use of logistic regression, this experiment is solving a non-convex problem. The results in Table 7 show that we can still obtain good results for a non-convex problem with different initialization, but it takes more time.

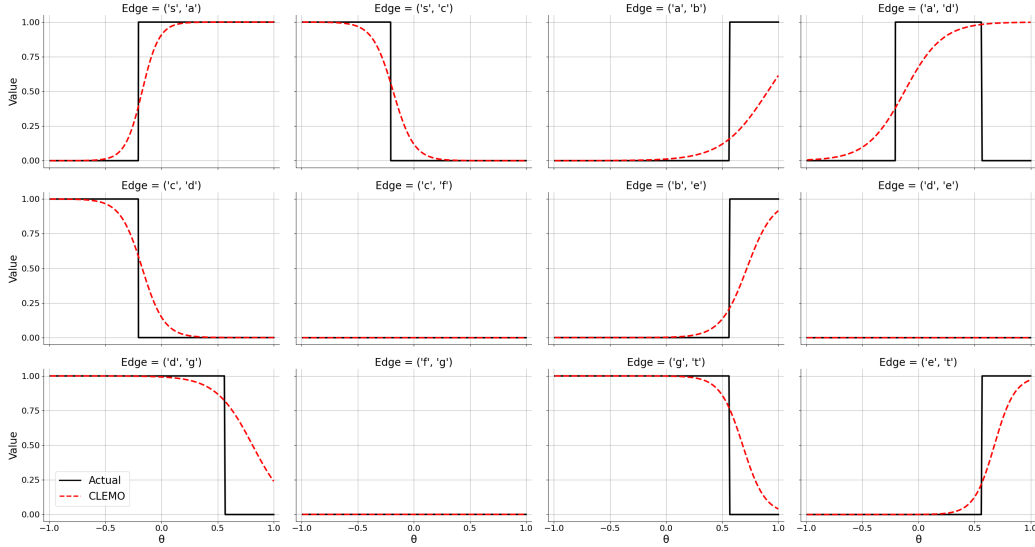
Table 7: Results of the Shortest Path Problem for the benchmark (LR) and CLEMO with various initializations.

Method	Infidelity: Objective value	Infidelity: Decision vector	Incoherence: Objective	Incoherence: Feasible Region	Time (s)
LR Benchmark	32.03	648.06	112.52	54.55	0.019
CLEMO (SLSQP) with warmstart	32.12	646.28	6.91	27.08	3.11
CLEMO (L-BFGS-B) with 0 initialization	32.15	658.85	9.12	21.66	92.3
CLEMO (L-BFGS-B) with 1 initialization	32.15	658.89	9.10	21.66	110.1
CLEMO (L-BFGS-B) with random initialization 1	32.08	662.62	5.64	21.82	118.67
CLEMO (L-BFGS-B) with random initialization 2	32.04	650.39	2.93	27.08	122.52
CLEMO (L-BFGS-B) with random initialization 3	32.05	650.20	3.38	27.21	85.61
CLEMO (L-BFGS-B) with random initialization 4	32.15	658.59	9.14	21.70	101.18
CLEMO (L-BFGS-B) with random initialization 5	32.11	661.49	7.27	21.83	72.23
CLEMO (L-BFGS-B) with random initialization 6	32.05	650.40	3.36	27.19	70.79
CLEMO (L-BFGS-B) with random initialization 7	32.04	650.10	2.94	27.13	104.33
CLEMO (L-BFGS-B) with random initialization 8	32.08	662.54	5.65	21.83	86.67
CLEMO (L-BFGS-B) with random initialization 9	32.04	649.80	2.94	27.18	94.54
CLEMO (L-BFGS-B) with random initialization 10	32.04	650.10	3.00	27.12	73.37

972 A.5 ADDITIONAL RESULTS EXPERIMENTS

973 A.5.1 SHORTEST PATH PROBLEM

974 For the SPP- θ considered in the experiments, we additionally present the prediction found by CLEMO
 975 for the decision vector compared to the values found by Dijkstra’s Algorithm in Fig. 4. In concordance
 976 with the results presented in the experiment section, we see CLEMO approximates the actual values
 977 relatively well.
 978
 979



982
983
984
985
986
987
988
989
990
991
992
993
994
995
996
997
998
999
1000 Figure 4: Decision variables of the shortest path of the SPP- θ instance as determined by Dijkstra’s
 1001 Algorithm and as predicted by CLEMO.

1002 A.5.2 KNAPSACK PROBLEM

1003 For the knapsack problem, we applied our method on 10 instances of each of the 4 types of problems
 1004 we considered. For each instance and for each method we used 10 different datasets to compare
 1005 our CLEMO with benchmark methods linear regression (LR) and decision tree regressor (DTR). In
 1006 Figs. 5 to 8 we present scatter plots of the total fidelity loss and total incoherence (both conditions
 1007 Eq. (3) and Eq. (4)) per instance and type of knapsack problem. Similar to the results presented in the
 1008 experiment section, we find that CLEMO significantly reduces incoherence while the faithfulness is
 1009 compromised relatively less.
 1010

1011 Next to the standard deviation of feature contribution, we consider an additional measure for stability,
 1012 the feature stability index (FSI). This is an adaptation of the variables stability index (VSI) as
 1013 presented in Visani et al. (2022). The higher this measure, the more the non-zero features found by
 1014 the different models due to resampling overlap. For a consistent explanation, the overlap should
 1015 be large. As we apply CLEMO on 10 different datasets for each instance of each type of knapsack
 1016 problem, we obtain 10 surrogate models given by $\beta_{CL}^1, \dots, \beta_{CL}^{10}$. We denote $\mathcal{F}_{k,j}^i$ for the set of
 1017 the top- k most contributing, non-zero features of the j -th component of β_{CL}^i . We define the (k, j) -
 1018 concordance of two models β^{i_1} and β^{i_2} as the size of the intersection between $\mathcal{F}_{k,j}^{i_1}$ and $\mathcal{F}_{k,j}^{i_2}$ divided
 1019 by the maximum potential overlap, *i.e.*,

$$1020 (k, j)\text{-concordance}(i_1, i_2) = \mathcal{F}_{k,j}^{i_1} \cap \mathcal{F}_{k,j}^{i_2} / k.$$

1021
 1022 Let us consider the k -feature stability index (k -FSI), which is the average (k, j) -concordance over all
 1023 pairs $\beta_{CL}^1, \dots, \beta_{CL}^{10}$ and all components j . Similar to VSI, k -FSI is bounded by 1 and the higher this
 1024 measure k -FSI, the more the different models agree on the top- k non-zero features of the different
 1025 components and hence the more stable the method is. Lastly, we define the FSI as the sum over k -FSI
 for $k = 1, \dots, 5$ resulting in a stability measure bounded by 5. When examining the FSI for CLEMO

and the benchmark methods in Table 2, we conclude that CLEMO has stability similar to the general linear regression approach.

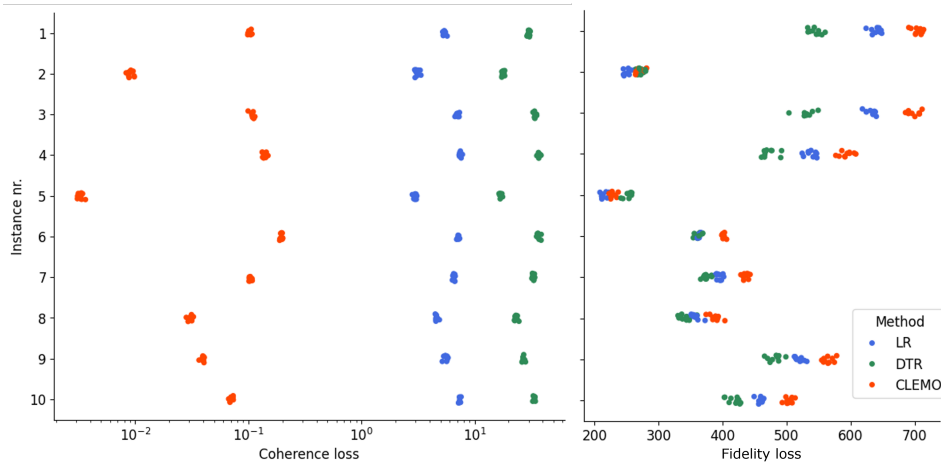


Figure 5: Scatter plot of the total incoherence (*i.e.*, coherence loss) and total fidelity losses as found by the different methods on 10 distinct sample sets per instance of the knapsack problem of type 1.

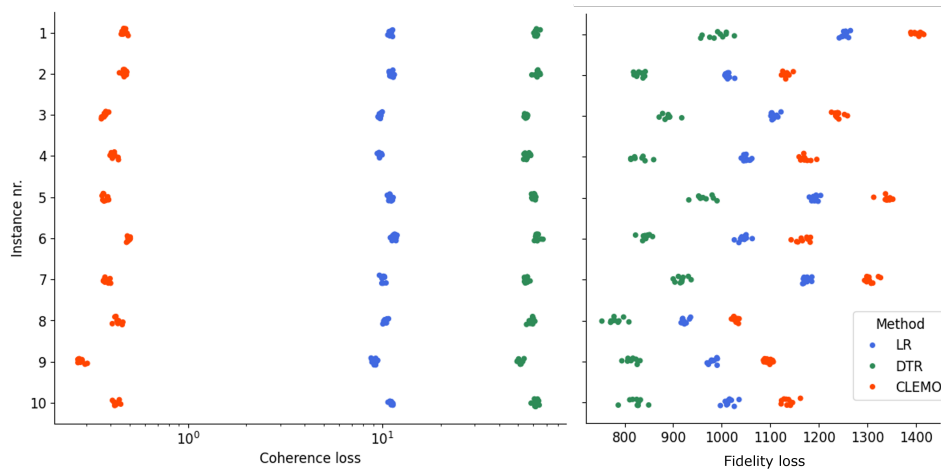
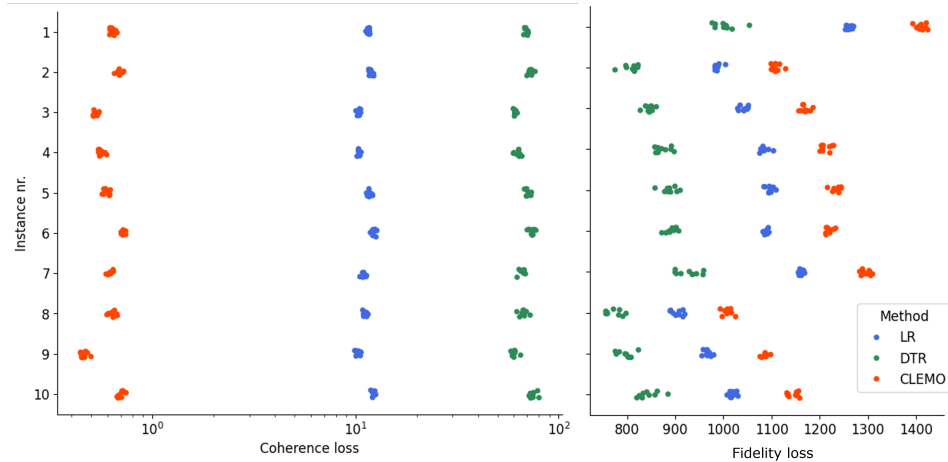


Figure 6: Scatter plot of the total incoherence (*i.e.*, coherence loss) and total fidelity losses as found by the different methods on 10 distinct sample sets per instance of the knapsack problem of type 2.

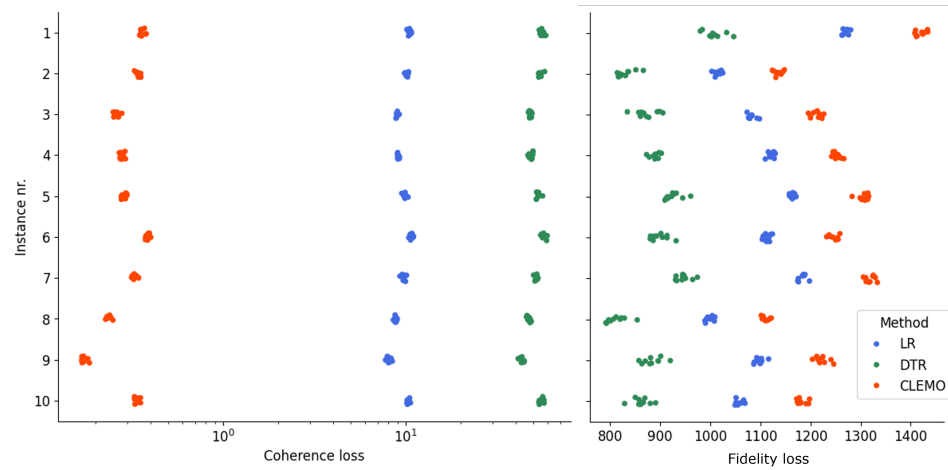
1080
 1081
 1082
 1083
 1084
 1085
 1086
 1087
 1088
 1089
 1090
 1091
 1092
 1093
 1094
 1095
 1096
 1097
 1098
 1099



1100
 1101
 1102
 1103
 1104
 1105
 1106
 1107
 1108
 1109
 1110
 1111

Figure 7: Scatter plot of the total incoherence (*i.e.*, coherence loss) and total fidelity losses as found by the different methods on 10 distinct sample sets per instance of the knapsack problem of type 3.

1112
 1113
 1114
 1115
 1116
 1117
 1118
 1119
 1120
 1121
 1122
 1123
 1124
 1125
 1126

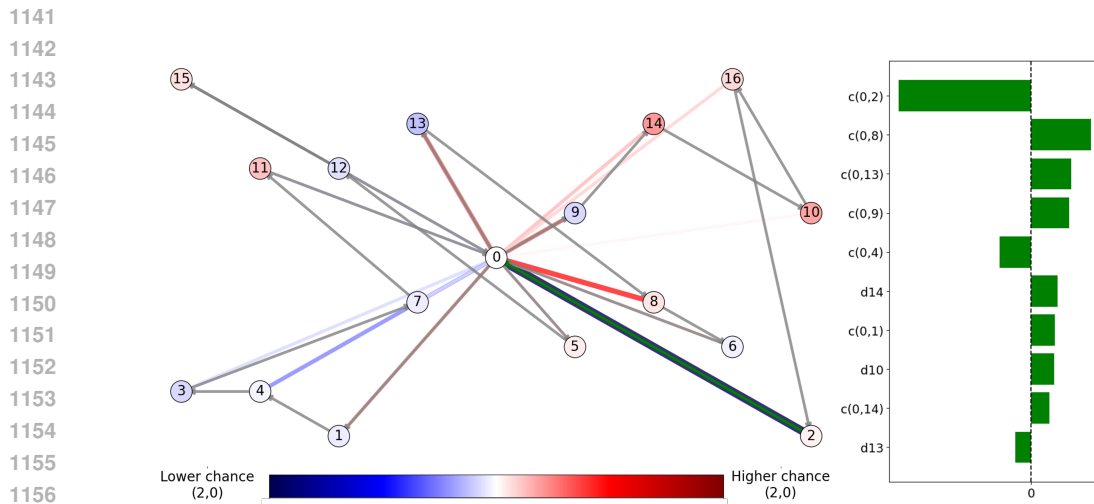


1127
 1128
 1129
 1130
 1131
 1132
 1133

Figure 8: Scatter plot of the total incoherence (*i.e.*, coherence loss) and total fidelity losses as found by the different methods on 10 distinct sample sets per instance of the knapsack problem of type 4.

1134 A.5.3 VEHICLE ROUTING PROBLEM

1135
1136 Similar to Fig. 3 as presented in Section 4, we display an additional explanation for the CVRP
1137 instance solved by Google OR-Tools. In Fig. 9, we see the explanation found by CLEMO for the
1138 decision variable x_{20} of the considered CVRP instance solved by Google OR-Tools. From this figure,
1139 a stakeholder can deduce that arc (2, 0) is less likely used by Google OR-Tools when c_{02} increases,
1140 but more likely when c_{08} increases.



1157 Figure 9: Explanation as found by CLEMO for the decision variable x_{20} visualized in the present
1158 problem network structure. Also, the top 10 relative feature contributions is depicted on the right.
1159

1160 A.6 STATEMENTS

1162 A.6.1 REPRODUCIBILITY STATEMENT

1164 In this work, we tried to achieve full reproducibility of the described methods and experiments by
1165 providing a link to our experiments on an anonymized GitHub: <https://anonymous.4open.science/r/CLEMO-899F>.
1166

1168 A.6.2 LLM STATEMENT

1169 In this work, Large Language Models were used solely to aid or polish writing. Concretely, we used
1170 these models to correct grammar and punctuation mistakes and to reformulate our original content to
1171 be more structured and clear.
1172
1173
1174
1175
1176
1177
1178
1179
1180
1181
1182
1183
1184
1185
1186
1187